



## Feature-based crystal construction in computer-aided nano-design

Cheng Qi, Yan Wang\*

Department of Industrial Engineering & Management Systems, University of Central Florida, 4000 Central Florida Blvd., Orlando, FL 32816-2993, USA

### ARTICLE INFO

#### Article history:

Received 11 June 2008

Accepted 12 December 2008

#### Keywords:

Feature based

Crystal construction

Feature operation

Periodic surface

Computer-aided nano-design

### ABSTRACT

Providing nanoengineers and scientists efficient and easy-to-use tools to create geometry conformations that have minimum energies is highly desirable in materials design. Recently we developed a periodic surface model to assist the construction of nanostructures parametrically for computer-aided nano-design. In this paper, we present a feature-based approach for crystal construction. The proposed approach creates models of basic features with the aid of periodic surfaces followed by operations between basic features. The goal is to introduce a rapid construction method for complex crystal structures.

© 2009 Elsevier Ltd. All rights reserved.

### 1. Introduction

Computer-aided nano-design (CAND) is an extension of computer-based engineering design traditionally at bulk scales to nanoscales. The general target of modeling and simulation in nanomaterials design is to search stable and realizable structures and conformations with the minimal total system energy. Geometry optimization is the central theme in most of the nanoscale simulations. For the widely used local search algorithms, simulation results are sensitively dependent on the initial conformation. Methods which allow for the efficient construction of initial geometries that are reasonably close to global optimal solutions are important to improve both convergence rate and accuracy of prediction. Thus, enabling efficient structural description and editing is one of the key research issues in CAND. At the molecular scale, parametric modeling mechanisms of particle aggregates are needed to support rapid construction and modification of geometries. At the mesoscale, super-porous structures with high surface-volume ratios in natural and man-made materials also need effective geometric descriptions.

With the observation that hyperbolic surfaces exist in nature ubiquitously and periodic features are common in condensed materials, we recently proposed an implicit surface modeling approach, periodic surface (PS), to represent geometric structures in nanoscales [1,2]. Periodic surfaces are either *loci* or *foci*. Loci surfaces are fictional continuous surfaces that pass through discrete particles in 3D space, whereas foci surfaces can be looked upon as isosurfaces of potential or density in which discrete particles are enclosed. The model allows for parametric construction from

atomic scale to mesoscale. Reconstruction of loci surfaces from crystals [3] and surface degree operations to support fine-grained modeling [4,5] were also studied.

In this paper, we propose a new feature-based approach to create crystal structures based on the PS model. Feature has been extensively used in traditional computer-aided design (CAD). It is the basic operational unit that has engineering or functional implications. We extend the previously developed PS geometric model and define nanoscale features, which represent some commonly used structures and patterns in materials design. This new feature-based crystal modeling approach is to increase the efficiency and convenience of crystal model construction, which is particularly important to design complex nanomaterial systems in the future.

The contributions of this paper include the unique way to create basic crystallographic features as the operational units using PS models. In addition, new feature operations are developed so that complex crystal structures such as polycrystalline and superlattice can be constructed efficiently. Moreover, the new feature-based approach also provides the convenience to modify a crystal structure parametrically.

In the remainder of the paper, Section 2 gives a brief overview of related work in molecular surface modeling and crystal representation. Section 3 describes the basis of the periodic surface model. Section 4 defines some basic features of PS models for crystals, and Section 5 presents methods of feature operations.

### 2. Molecular surface modeling and crystal representation

For visualization purpose, there has been some research on molecular surface modeling to visualize molecular structures [6]. Lee and Richards [7] first introduced solvent-accessible surface, the locus of a probe rolling over van der Waals surface, to represent

\* Corresponding author. Tel.: +1 407 823 5568; fax: +1 407 823 3413.  
E-mail addresses: [cqi@mail.ucf.edu](mailto:cqi@mail.ucf.edu) (C. Qi), [wangyan@mail.ucf.edu](mailto:wangyan@mail.ucf.edu) (Y. Wang).

the boundary of molecules. Connolly [8] presented an analytical method to calculate the surface. Recently, Carson [9] represented molecular surfaces with B-spline wavelets. Edelsbrunner [10] described molecules with implicit-form skin surfaces. Bajaj et al. [11] represented solvent-accessible surfaces by NURBS (non-uniform rational B-spline). Au and Woo [12] studied the topological changes of macromolecules during folding with the aid of ribbons. Ryu et al. [13] constructed NURBS molecular surfaces with the aid of Euclidean Voronoi diagrams. Zhang et al. [14] constructed implicit solvation surfaces from the Gaussian kernel. These research efforts concentrate on visualization of molecules, whereas construction support of molecular and atomic structures for design purpose are not considered. We recently proposed a periodic surface model to construct nanostructures parametrically. In this paper, a feature-based approach to parametrically construct crystal structures is proposed.

For 3D crystals, a point group is a set of symmetry operations including reflection, rotation, inversion and improper rotation (inversion after rotation) which leave at least one point fixed and the appearance of the crystal structure unchanged. The total number of point groups is 32, each of which is uniquely symbolized in crystallography. A crystal class is a set of crystals which have the same point group. Based on the number and type of symmetry axes for symmetry operations, the 32 point groups are divided into seven categories. Each category is corresponding to one of the seven crystal systems (cubic, orthorhombic, tetragonal, triclinic, monoclinic, rhombohedral and hexagonal) in space lattices, which describe the translational symmetry (the translation operation does not change crystal structures). There are totally fourteen possible unique space lattices. They are called Bravais lattices. Each lattice point on Bravais lattices may represent a motif, which is a set of atoms arranged in a particular way. The combination of the 32 point groups with the fourteen Bravais lattices forms 230 space groups which are operations of both symmetry operations and translations. The fourteen Bravais lattices are represented by lattice parameters. They are the lengths of edges of the unit cell  $a, b, c$ , and the angles between them  $\alpha, \beta, \gamma$  [15,16].

In the existing material simulation software, Bravais lattices are used to directly create crystal structures. Users need to specify the desired space lattice and its lattice parameters. Because the lattice points of the fourteen Bravais lattices are known, once the lattice parameters are determined, users do not have to specify the  $x, y$  and  $z$  coordinates of the lattice points for simple and small crystals. The lattices are thus generated periodically by the software. For example, for a face-centered cubic (as also shown in Fig. 2), the number of lattice points per unit cell is four, and their positions are  $(0,0,0), (0, 1/2, 1/2), (1/2, 0, 1/2)$  and  $(1/2, 1/2, 0)$ . The user specifies the values of  $a, b, c, \alpha, \beta$ , and  $\gamma$  as 1, 1, 1,  $90^\circ, 90^\circ$  and  $90^\circ$ . The software locates the four lattice points and repeats them periodically based on the lattice parameters. However, this method is not efficient for large and complex crystals because the  $x, y$  and  $z$  coordinates of motifs in a unit cell need to be specified one by one manually. Moreover, this explicit construction approach is not flexible for modifications when positions need to be changed. In this paper, we propose a feature-based approach based on PS models so that complex structures can be constructed by operations on one or more features. This approach avoids specifying the coordinates manually so that complex crystal systems are easy to be built and modified.

### 3. Periodic surface

A periodic surface (PS) is generally defined as

$$\psi(\mathbf{r}) = \sum_{l=1}^L \sum_{m=1}^M \mu_{lm} \cos(2\pi\kappa_l(\mathbf{p}_m^T \cdot \mathbf{r})) = 0 \quad (1)$$

where  $\kappa_l$  is the scale parameter,  $\mathbf{p}_m = [a_m, b_m, c_m, \theta_m]^T$  is a basis vector, such as one of

$$\{\mathbf{e}_0, \mathbf{e}_1, \mathbf{e}_2, \mathbf{e}_3, \mathbf{e}_4, \mathbf{e}_5, \mathbf{e}_6, \mathbf{e}_7, \mathbf{e}_8, \mathbf{e}_9, \mathbf{e}_{10}, \mathbf{e}_{11}, \mathbf{e}_{12}, \mathbf{e}_{13}, \dots\} \\ = \left\{ \begin{bmatrix} 0 \\ 0 \\ 0 \\ 1 \end{bmatrix}, \begin{bmatrix} 1 \\ 0 \\ 0 \\ 1 \end{bmatrix}, \begin{bmatrix} 0 \\ 1 \\ 0 \\ 1 \end{bmatrix}, \begin{bmatrix} 0 \\ 0 \\ 1 \\ 1 \end{bmatrix}, \begin{bmatrix} 1 \\ 1 \\ 0 \\ 1 \end{bmatrix}, \begin{bmatrix} 1 \\ 0 \\ 1 \\ 1 \end{bmatrix}, \begin{bmatrix} 1 \\ 1 \\ 1 \\ 1 \end{bmatrix}, \begin{bmatrix} 0 \\ 1 \\ 1 \\ 1 \end{bmatrix}, \begin{bmatrix} 1 \\ 1 \\ 1 \\ 1 \end{bmatrix} \right\} \\ \times \left\{ \begin{bmatrix} 1 \\ -1 \\ 0 \\ 1 \end{bmatrix}, \begin{bmatrix} -1 \\ 0 \\ 1 \\ 1 \end{bmatrix}, \begin{bmatrix} 0 \\ 1 \\ -1 \\ 1 \end{bmatrix}, \begin{bmatrix} 1 \\ -1 \\ 1 \\ 1 \end{bmatrix}, \begin{bmatrix} -1 \\ 1 \\ 1 \\ 1 \end{bmatrix}, \begin{bmatrix} 1 \\ 1 \\ -1 \\ 1 \end{bmatrix}, \dots \right\}, \quad (2)$$

which represents a basis plane in the 3-space  $E^3$ ,  $\mathbf{r} = [x, y, z, w]^T$  is the location vector with homogeneous coordinates, and  $\mu_{lm}$  is the periodic moment. We usually assume that  $w = 1$  if not explicitly specified. The degree of  $\psi(\mathbf{r})$  in Eq. (1) is defined as the number of unique periodic basis vectors in the set  $\{\mathbf{p}_m\}$ ,  $\text{deg}(\psi(\mathbf{r})) := |\{\mathbf{p}_m\}|$ . The scale of  $\psi(\mathbf{r})$  is defined as the number of unique scale parameters in the set  $\{\kappa_l\}$ ,  $\text{sca}(\psi(\mathbf{r})) := |\{\kappa_l\}|$ . We usually assume that the scale parameters are natural numbers ( $\kappa_l \in N$ ). Each basis vector can be regarded as a set of parallel 2D subspaces in  $E^3$ , which plays an important role in interactive manipulation of PS models.

The locations of atoms or particles in the  $E^3$  space can be determined by their simultaneous appearance in three or more subspaces defined by periodic surfaces. Tiling is the process of regularly subdividing and discretizing the space. One of the approaches for tiling is by intersection. Finding the intersection among  $\psi_1(\mathbf{r}) = 0, \psi_2(\mathbf{r}) = 0$ , and  $\psi_3(\mathbf{r}) = 0$  is to solve the constraint.

$$\psi(\mathbf{r}) = \psi_1^2(\mathbf{r}) + \psi_2^2(\mathbf{r}) + \psi_3^2(\mathbf{r}) = 0. \quad (3)$$

For example,  $P$  surfaces (as illustrated in Fig. 1(b)) can be used to build cage-like structures, such as Sodalite minerals, which are widely used as molecular sieves and catalysts in pollution control, detergent, manufacturing, and other fields. Fig. 1 illustrates tiling by intersection between a  $P$  surface with two Grid surfaces to create a Sodalite framework.

### 4. Basic features

Here, the basic features we define are Bravais lattices. The basic features are the fundamental building blocks for complex structures. They are simple cubic, body-centered cubic, face-centered cubic, simple orthorhombic, base-centered orthorhombic, body-centered orthorhombic, face-centered orthorhombic, simple tetragonal, body-centered tetragonal, simple monoclinic, base-centered monoclinic, triclinic, rhombohedral and hexagonal. All crystalline materials recognized until now (not including quasicrystals) fit in one of these arrangements.

Consider the basic features in a unit block domain

$$D_1 = [-0.5 \leq x \leq 0.5, -0.5 \leq y \leq 0.5, -0.5 \leq z \leq 0.5, 1]. \quad (4)$$

By means of the intersection operation among three periodic surfaces, all of the fourteen basic features can be built as shown in Fig. 2.

Table 1 lists the corresponding PS models of the fourteen basic features. Feature A is called an extended feature of Feature B if the lattice points in B is a subset of the ones in A. Body-centered, face-centered and base-centered features are extended features from a simple basic feature, and they are in the same category as that of the simple basic feature. A simple basic feature can be simple cubic, simple orthorhombic, simple tetragonal or simple monoclinic. The fourteen basic features are then grouped into seven categories which are cubic, orthorhombic, tetragonal, monoclinic, triclinic, rhombohedral and hexagonal. As can be seen, the degree of each periodic surface is one so that all of these basic features could be represented by intersections among three periodic planes in

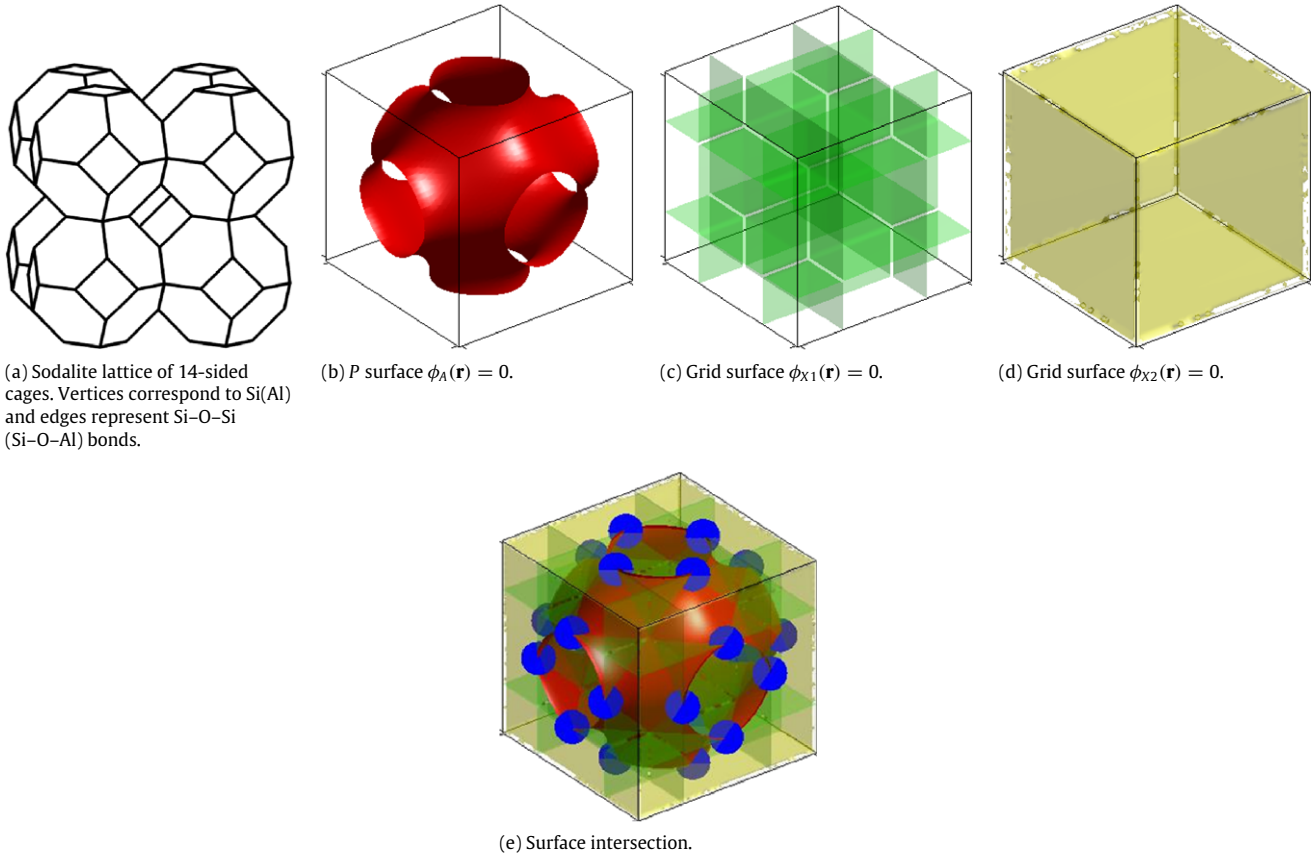


Fig. 1. Tiling by intersection of  $P$  surface with Grid surfaces to create Sodalite framework.

Table 1

Periodic surface models of the fourteen basic crystal features.

Crystal structure	Implicit periodic surface model
Simple cubic	$\cos^2(\pi x) + \cos^2(\pi y) + \cos^2(\pi z) = 0$
Body-centered cubic	$\cos^2(\pi(x - y + 0.5)) + \cos^2(\pi(x + y + 0.5)) + \cos^2(\pi(y + z + 0.5)) = 0$
Face-centered cubic	$\cos^2(\pi(x + y + z)) + \cos^2(\pi(-x + y + z)) + \cos^2(\pi(-x - y + z)) = 0$
Simple orthorhombic	$\cos^2(\pi x/a) + \cos^2(\pi y/b) + \cos^2(\pi z/c) = 0, a \neq b \neq c$
Base-centered orthorhombic	$\cos^2(\pi(x/a - y/b + 0.5)) + \cos^2(\pi(x/a + y/b + 0.5)) + \cos^2(\pi z/c) = 0, a \neq b \neq c$
Body-centered orthorhombic	$\cos^2(\pi(x/a - y/b + 0.5)) + \cos^2(\pi(x/a + y/b + 0.5)) + \cos^2(\pi(y/b + z/c + 0.5)) = 0, a \neq b \neq c$
Face-centered orthorhombic	$\cos^2(\pi(x/a + y/b + z/c)) + \cos^2(\pi(-x/a + y/b + z/c)) + \cos^2(\pi(-x/a - y/b + z/c)) = 0, a \neq b \neq c$
Simple tetragonal	$\cos^2(\pi x/a) + \cos^2(\pi y/a) + \cos^2(\pi z/c) = 0, a \neq c$
Body-centered tetragonal	$\cos^2(\pi(x/a - y/a + 0.5)) + \cos^2(\pi(x/a + y/a + 0.5)) + \cos^2(\pi(y/a + z/c + 0.5)) = 0, a \neq c$
Simple monoclinic	$\cos^2(\pi(-x/(1 - \text{ctg}\alpha) + z/(\text{tg}\alpha - 1))) + \cos^2(\pi y) + \cos^2(\pi z) = 0, \alpha \neq 90^\circ$
Base-centered monoclinic	$\cos^2(2\pi(x/(\text{ctg}\alpha - 1) + z/(\text{tg}\alpha - 1) + 0.75)) + \cos^2(\pi(x/(1 - \text{ctg}\alpha) + y - z/(\text{tg}\alpha - 1) + 0.5)) + \cos^2(\pi z) = 0, \alpha \neq 90^\circ$
Triclinic	$\cos^2\left[\frac{\pi}{\sin\gamma - \cos\gamma - k_1}(x \sin\gamma + y \cos\gamma - zk_1)\right] + \cos^2\left[\frac{\pi}{k_2 - 1}(-y + zk_2)\right] + \cos^2(\pi z) = 0, \alpha, \beta, \gamma \neq 90^\circ$ $k_1 = \frac{\cos\alpha + \cos\beta \cos\gamma}{\sqrt{[\cos\beta + \cos(\alpha - \gamma)][\cos\beta + \cos(\alpha + \gamma)]}}, k_2 = \frac{\cos\beta + \cos\alpha \cos\gamma}{\sqrt{[\cos\beta + \cos(\alpha - \gamma)][\cos\beta + \cos(\alpha + \gamma)]}}$
Rhombohedral	$\cos^2\left[\pi(x/a + y/a \tan\gamma - zk_1/a \sin\lambda)\right] + \cos^2\left[\frac{\pi}{a \sin\gamma}(-y + zk_2)\right] + \cos^2\left[\frac{\pi zk_2 \sin\gamma}{a(\cos\beta + \cos\alpha \cos\gamma)}\right] = 0, \alpha, \beta, \gamma \neq 90^\circ$ $k_1 = \frac{\cos\alpha + \cos\beta \cos\gamma}{\sqrt{[\cos\beta + \cos(\alpha - \gamma)][\cos\beta + \cos(\alpha + \gamma)]}}, k_2 = \frac{\cos\beta + \cos\alpha \cos\gamma}{\sqrt{[\cos\beta + \cos(\alpha - \gamma)][\cos\beta + \cos(\alpha + \gamma)]}}$
Hexagonal	$\cos^2(\pi(2x/\sqrt{3}a + 0.5)) + \cos^2(\pi y/c) + \cos^2(\pi(x/\sqrt{3}a + z/a + 0.5)) = 0, a \neq c$

$E^3$  space. Transformation operations [3] on a single periodic surface, such as rotation, translation and scaling, can be applied to adjust the positions.

Simultaneous transformation operations of the three periodic planes are equivalent to applying the operations to the corresponding basic feature.

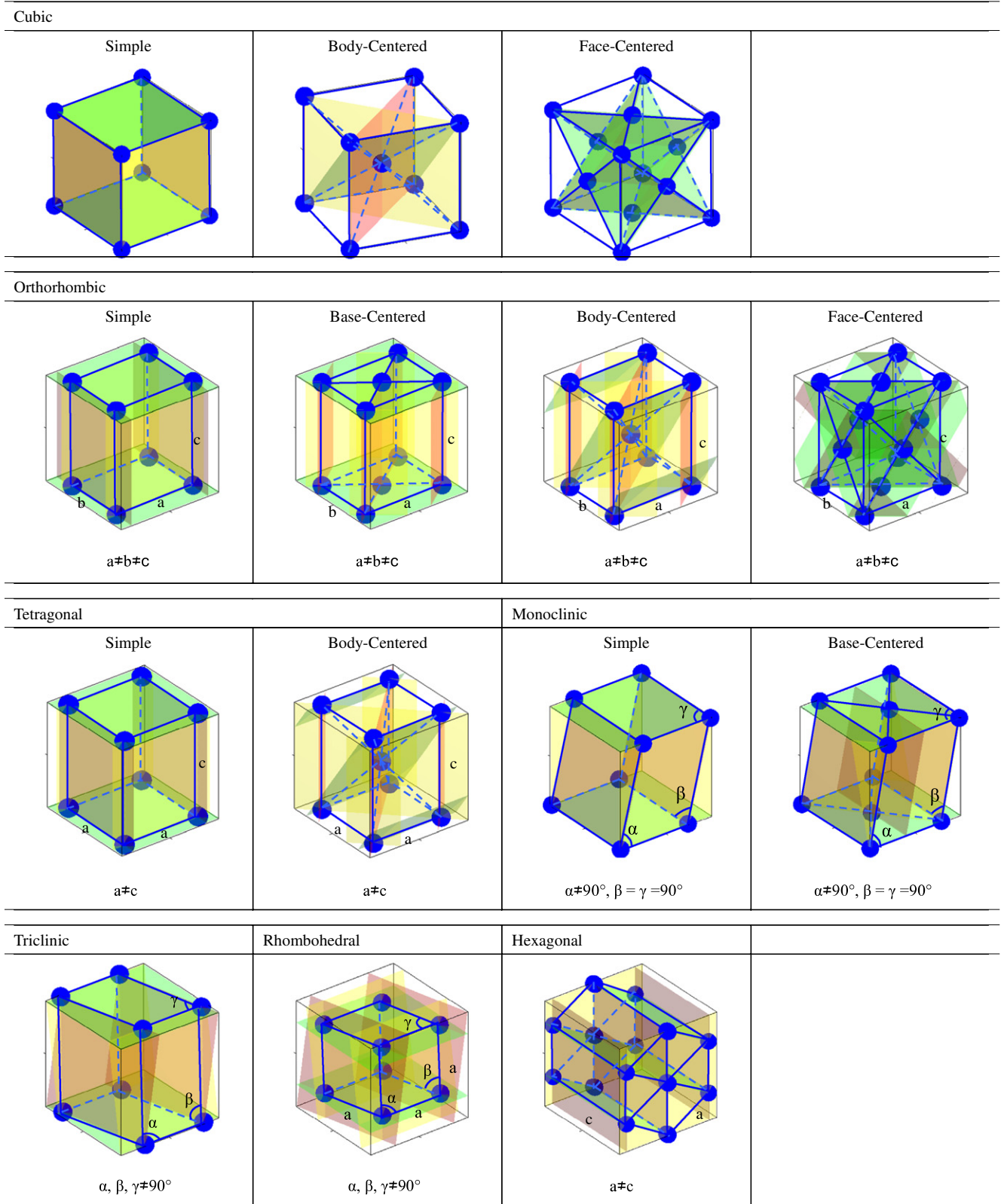


Fig. 2. Fourteen basic crystal features.

## 5. Feature operations

In previous work [1,2], approaches of particles tiling such as loci surface intersection were discussed. In this section, we extend the tiling to feature-based operations to rapidly locate particles in crystal structures. The new feature-based approach provides

a more efficient way to create crystal structures than direct loci surface intersection, especially when structures become complex and the number of loci surfaces increases accordingly.

The feature operations that are described here include: center symmetry, translation, scaling, masking, demasking, imposing, union and insertion.

### 5.1. Center symmetry

Let  $\mathbf{S}_{\text{sym}} = \begin{bmatrix} -1 & 0 & 0 & 0 \\ 0 & -1 & 0 & 0 \\ 0 & 0 & -1 & 0 \\ 0 & 0 & 0 & 1 \end{bmatrix}$  be the center reflection

transformation matrix, which is symmetric, orthonormal, and self-inverse, i.e.  $\mathbf{S}_{\text{sym}} = \mathbf{S}_{\text{sym}}^T = \mathbf{S}_{\text{sym}}^{-1}$ . The center symmetry operation of a feature  $\psi(\mathbf{r}) = \psi_1^2(\mathbf{r}) + \psi_2^2(\mathbf{r}) + \psi_3^2(\mathbf{r}) = 0$  is defined as

$$T_{\text{sym}}[\psi(\mathbf{r})] := \psi(\mathbf{S}_{\text{sym}}^{-1} \cdot \mathbf{r}). \quad (5)$$

**Lemma 1.** The fourteen basic features in Table 1 are self-center symmetric.

**Proof.** Apply the center symmetric transformation to the surface models in Table 1, we receive

$$\begin{aligned} T_{\text{sym}}[\psi(\mathbf{r})] &= \psi_1^2(\mathbf{S}_{\text{sym}}^{-1} \cdot \mathbf{r}) + \psi_2^2(\mathbf{S}_{\text{sym}}^{-1} \cdot \mathbf{r}) + \psi_3^2(\mathbf{S}_{\text{sym}}^{-1} \cdot \mathbf{r}) \\ &= \cos^2(2\pi\kappa_{l1}(\mathbf{p}_{m1}^T \cdot \mathbf{S}_{\text{sym}}^{-1} \cdot \mathbf{r})) \\ &\quad + \cos^2(2\pi\kappa_{l2}(\mathbf{p}_{m2}^T \cdot \mathbf{S}_{\text{sym}}^{-1} \cdot \mathbf{r})) \\ &\quad + \cos^2(2\pi\kappa_{l3}(\mathbf{p}_{m3}^T \cdot \mathbf{S}_{\text{sym}}^{-1} \cdot \mathbf{r})) \\ &= \cos^2(2\pi\kappa_{l1}(-\mathbf{p}_{m1}^T \cdot \mathbf{r})) + \cos^2(2\pi\kappa_{l2}(-\mathbf{p}_{m2}^T \cdot \mathbf{r})) \\ &\quad + \cos^2(2\pi\kappa_{l3}(-\mathbf{p}_{m3}^T \cdot \mathbf{r})) \\ &= \cos^2(2\pi\kappa_{l1}(\mathbf{p}_{m1}^T \cdot \mathbf{r})) + \cos^2(2\pi\kappa_{l2}(\mathbf{p}_{m2}^T \cdot \mathbf{r})) \\ &\quad + \cos^2(2\pi\kappa_{l3}(\mathbf{p}_{m3}^T \cdot \mathbf{r})) \\ &= \psi(\mathbf{r}). \end{aligned}$$

Therefore, the fourteen basic features are self-center symmetric.  $\square$

### 5.2. Translation

Given a basic feature  $\psi(\mathbf{r}) = \psi_1^2(\mathbf{r}) + \psi_2^2(\mathbf{r}) + \psi_3^2(\mathbf{r}) = 0$ , the translation operation is defined as

$$T_{\text{tran}}[\psi(\mathbf{r}), \mathbf{r}_1] = \psi(\mathbf{r} - \mathbf{r}_1) = \psi(\mathbf{T}^{-1} \cdot \mathbf{r}) \quad (6)$$

which is equivalent to translating periodic surfaces  $\psi_1(\mathbf{r})$ ,  $\psi_2(\mathbf{r})$  and  $\psi_3(\mathbf{r})$  simultaneously, where

$$\mathbf{T} = \begin{bmatrix} 1 & 0 & 0 & t_x \\ 0 & 1 & 0 & t_y \\ 0 & 0 & 1 & t_z \\ 0 & 0 & 0 & 1 \end{bmatrix}, \quad (\mathbf{T}^{-1})^T = \begin{bmatrix} 1 & 0 & 0 & 0 \\ 0 & 1 & 0 & 0 \\ 0 & 0 & 1 & 0 \\ -t_x & -t_y & -t_z & 1 \end{bmatrix},$$

$$\mathbf{r}_1 = \begin{bmatrix} t_x \\ t_y \\ t_z \\ 1 \end{bmatrix}.$$

### 5.3. Scaling

Given a basic feature  $\psi(\mathbf{r}) = \psi_1^2(\mathbf{r}) + \psi_2^2(\mathbf{r}) + \psi_3^2(\mathbf{r}) = 0$ , the scaling operation is defined as

$$T_{\text{scal}}[\psi(\mathbf{r}), s_x, s_y, s_z] = \psi(\mathbf{S}^{-1} \cdot \mathbf{r}) \quad (7)$$

which is equivalent to scaling the periodic surfaces  $\psi_1(\mathbf{r})$ ,  $\psi_2(\mathbf{r})$  and  $\psi_3(\mathbf{r})$  simultaneously, where

$$\mathbf{S} = \mathbf{S}^T = \begin{bmatrix} s_x & 0 & 0 & 0 \\ 0 & s_y & 0 & 0 \\ 0 & 0 & s_z & 0 \\ 0 & 0 & 0 & 1 \end{bmatrix},$$

$$\text{and } \mathbf{S}^{-1} = \begin{bmatrix} 1/s_x & 0 & 0 & 0 \\ 0 & 1/s_y & 0 & 0 \\ 0 & 0 & 1/s_z & 0 \\ 0 & 0 & 0 & 1 \end{bmatrix}.$$

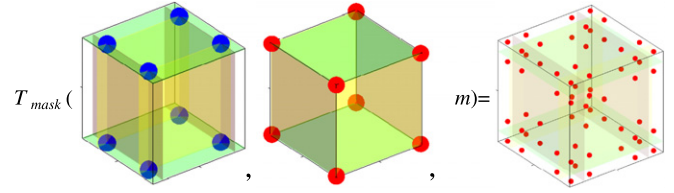


Fig. 3. A tetragonal masked by a simple cubic ( $m = 5$ ).

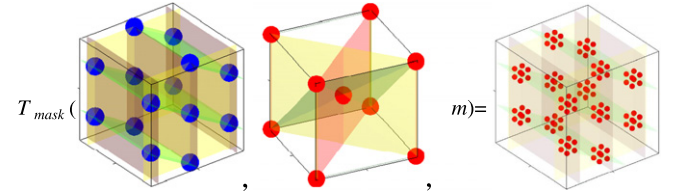


Fig. 4. A hexagonal masked by a body-centered cubic ( $m = 10$ ).

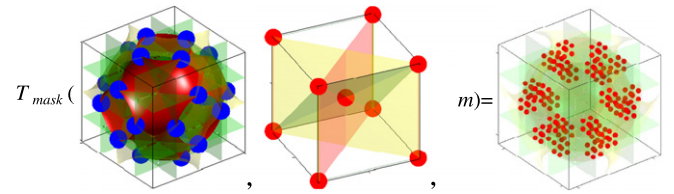


Fig. 5. Sodalite framework masked by a body-centered cubic ( $m = 10$ ).

### 5.4. Masking

It is known in crystallography that each lattice point of a Bravais lattice represents the same group of atoms which fit in one of the fourteen Bravais lattices in a smaller scale. That is, each lattice point of Bravais lattices can be further expanded and becomes a unit of the lattice itself. Therefore, we propose a masking operation to support such a structure expansion.

Given basic features  $\psi_A(\mathbf{r}') = \psi_{11}^2(\mathbf{r}') + \psi_{12}^2(\mathbf{r}') + \psi_{13}^2(\mathbf{r}') = 0$  and  $\psi_B(\mathbf{r}') = \psi_{21}^2(\mathbf{r}') + \psi_{22}^2(\mathbf{r}') + \psi_{23}^2(\mathbf{r}') = 0$  in the domain  $D_1$ , the masking operation is defined as

$$T_{\text{mask}}[\psi_A(\mathbf{r}'), \psi_B(\mathbf{r}'), m](\mathbf{r}) := \psi_A(\mathbf{r}') + T_{\text{sym}}[T_{\text{tran}}[T_{\text{scal}}[\psi_B(\mathbf{r}'), m, m, m], \mathbf{r}]] \quad (8)$$

where  $\psi_A(\mathbf{r}')$  is the *main feature*,  $\psi_B(\mathbf{r}')$  is the *mask feature* and  $m$  is the *mask index*. The operation of masking expands each lattice point of the basic feature  $\psi_A(\mathbf{r}')$ , each of which becomes the basic feature  $\psi_B(\mathbf{r}')$ . Figs. 3 and 4 illustrate the feature expansion effect of the masking operation.

The masking operation can also be applied when the main feature is any structure other than a basic feature. Fig. 5 illustrates the effect of the masking operation between a Sodalite framework and a body-centered cubic.

**Lemma 2.** The scaling operation of a masked structure is equivalent to the masking operation applied to both of the scaled main feature and the scaled mask feature by the same scaling operation.

**Proof.**

$$\begin{aligned} T_{\text{scal}}[T_{\text{mask}}[\psi_A(\mathbf{r}'), \psi_B(\mathbf{r}'), m, m, m](\mathbf{r}), s_x, s_y, s_z] \\ &= T_{\text{scal}}[\psi_A(\mathbf{r}') + T_{\text{sym}}[T_{\text{tran}}[T_{\text{scal}}[\psi_B(\mathbf{r}'), m, m, m], \mathbf{r}]], s_x, s_y, s_z] \\ &= T_{\text{scal}}[\psi_A(\mathbf{r}'), s_x, s_y, s_z] \\ &\quad + T_{\text{scal}}[T_{\text{sym}}[T_{\text{tran}}[T_{\text{scal}}[\psi_B(\mathbf{r}'), m, m, m], \mathbf{r}]], s_x, s_y, s_z] \\ &= \psi_A(\mathbf{S}^{-1} \cdot \mathbf{r}') + T_{\text{sym}}[T_{\text{tran}}[T_{\text{scal}}[\psi_B(\mathbf{S}^{-1} \cdot \mathbf{r}'), m, m, m], \mathbf{r}]] \\ &= T_{\text{mask}}[T_{\text{scal}}[\psi_A(\mathbf{r}'), s_x, s_y, s_z], \\ &\quad T_{\text{scal}}[\psi_B(\mathbf{r}'), s_x, s_y, s_z], m, m, m](\mathbf{r}). \quad \square \end{aligned}$$

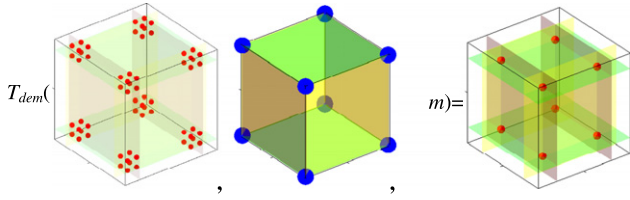


Fig. 6. Demasking operation by a simple cubic ( $m = 10$ ).

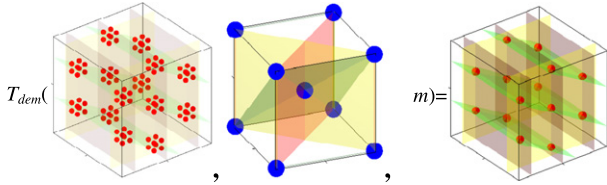


Fig. 7. Demasking operation by a body-centered cubic ( $m = 10$ ).

### 5.5. Demasking

Given an original structure  $\psi_A(\mathbf{r}')$  and a mask feature  $\psi_B(\mathbf{r}') = \psi_{21}^2(\mathbf{r}') + \psi_{22}^2(\mathbf{r}') + \psi_{23}^2(\mathbf{r}') = 0$ , a demasking operation is defined as

$$T_{\text{mask}}[\psi_A(\mathbf{r}'), \psi_B(\mathbf{r}'), m](\mathbf{r}) := \psi_A(\mathbf{r}') + T_{\text{sym}}[T_{\text{tran}}[T_{\text{scal}}[\psi_B(\mathbf{r}'), m, m, m], \mathbf{r}]] \quad (9)$$

where  $m$  is the demasking index. The operation of demasking collapses any of the mask feature  $\psi_B(\mathbf{r}')$  which is available in the structure  $\psi_A(\mathbf{r}')$  into a single lattice point. The demasking operation can be looked upon as the inverse operation of the masking operation. Figs. 6 and 7 illustrate the feature collapse effect of the demasking operation.

**Lemma 3.** *The demasking operation collapses not only the mask feature but also its extended features which are available in the original feature.*

**Proof.** Assume that  $\psi_A(\mathbf{r}')$  is an original structure and  $\psi_{B1}(\mathbf{r}')$  is an extended feature of a mask feature  $\psi_B(\mathbf{r}')$ . Since  $\psi_B(\mathbf{r}')$  is a subset of  $\psi_{B1}(\mathbf{r}')$ ,  $\forall \mathbf{r}, \psi_B(\mathbf{r}') = 0 \Rightarrow \psi_{B1}(\mathbf{r}') = 0$ . Therefore,

$$\begin{aligned} T_{\text{dem}}[\psi_A(\mathbf{r}'), \psi_{B1}(\mathbf{r}'), m](\mathbf{r}) &= \{\mathbf{r} | \forall \mathbf{r}', T_{\text{tran}}[T_{\text{scal}}[\psi_{B1}(\mathbf{r}'), m, m, m], \mathbf{r}] = 0, \psi_A(\mathbf{r}') = 0\} \\ &\subseteq \{\mathbf{r} | \forall \mathbf{r}', T_{\text{tran}}[T_{\text{scal}}[\psi_B(\mathbf{r}'), m, m, m], \mathbf{r}] = 0, \\ &\quad \psi_A(\mathbf{r}') = 0\} = T_{\text{dem}}[\psi_A(\mathbf{r}'), \psi_B(\mathbf{r}'), m](\mathbf{r}). \quad \square \end{aligned}$$

Fig. 8 illustrates the subset effect of demasking. An expanded structure is created by masking a hexagonal with a body-centered cubic. When the expanded structure is demasked by a simple cubic, the hexagonal can be recovered.

### 5.6. Impose

Given two basic features  $\psi_A(\mathbf{r}) = \psi_{11}^2(\mathbf{r}) + \psi_{12}^2(\mathbf{r}) + \psi_{13}^2(\mathbf{r}) = 0$  and  $\psi_B(\mathbf{r}) = \psi_{21}^2(\mathbf{r}) + \psi_{22}^2(\mathbf{r}) + \psi_{23}^2(\mathbf{r}) = 0$  in the domain  $D_1$ , the impose operation is defined as

$$T_{\text{imp}}[\psi_A(\mathbf{r}), \psi_B(\mathbf{r})] := \psi_A(\mathbf{r}) \cdot \psi_B(\mathbf{r}). \quad (10)$$

The impose operation overlaps one feature onto another one. Fig. 9 illustrates the feature overlap effect of the impose operation.

A diamond structure can be created by an impose operation between two face-centered cubics, one of which is translated along  $x$ ,  $y$  and  $z$  directions. More specifically, if  $\psi(\mathbf{r})$  is a face-centered cubic structure, a diamond structure can be constructed

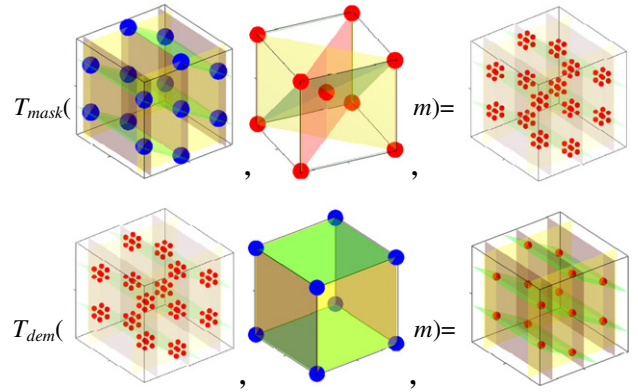


Fig. 8. An example of the subset effect in Lemma 3 ( $m = 10$ ).

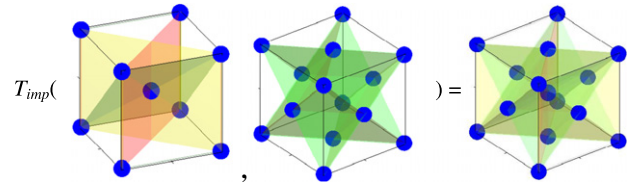


Fig. 9. A body-centered cubic imposed by a face-centered cubic.

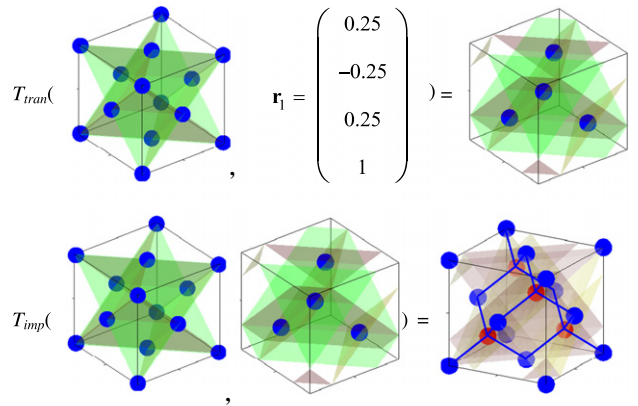


Fig. 10. An illustration of the construction of the diamond structure.

by  $T_{\text{imp}}[\psi(\mathbf{r}), T_{\text{tran}}[\psi(\mathbf{r}), \mathbf{r}_1]]$ , where  $\mathbf{r}_1 = (0.25, -0.25, 0.25, 1)^T$ . Fig. 10 illustrates the construction of the diamond lattice.

It is easy to verify that a basic feature keeps itself unchanged after an impose operation with itself. An extended basic feature keeps itself unchanged after an impose operation with a simple basic feature in the same category. Scaling an imposed structure is equivalent to imposing two scaled features.

### 5.7. Union

The union operation joins two basic features in the same category. By union of two basic features, the two are joined together by sharing lattice positions on their edge cut surfaces. Fig. 11 illustrates the union operation between two features, where the red block and the blue block represent the two basic features. Joined by the union operation, the two features are mixed and appear periodically in 3D space. It is obvious that the union of a basic feature with itself keeps the feature unchanged.

Notice that if the structure in Fig. 11 is demasked by the red block, the result of this demasking operation is a face-centered basic feature if the red block is not a subset of the blue block. Based on this observation, we generalize the definition of the union operation as follows. If  $\psi_C(\mathbf{r})$  is the face-centered basic feature in

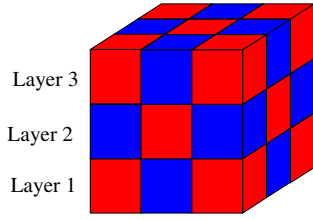


Fig. 11. An illustration of union operation.

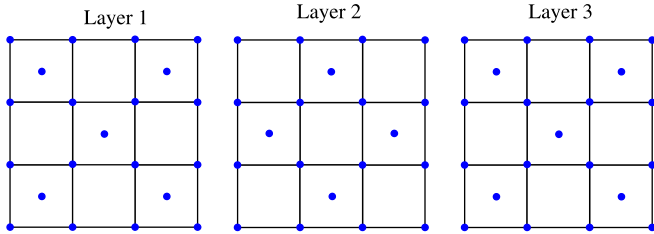


Fig. 12. A three-layer view of the union structure in Fig. 11.

the same category as the basic features  $\psi_A(\mathbf{r})$  and  $\psi_B(\mathbf{r})$  ( $\psi_A(\mathbf{r}) \neq \psi_B(\mathbf{r})$ ), the union operation is defined as

$$T_{un}[\psi_A(\mathbf{r}), \psi_B(\mathbf{r})] := T_{mask}[\psi_C(\mathbf{r}), T_{imp}[\psi_A(\mathbf{r}), \psi_B(\mathbf{r})], 2]. \quad (11)$$

Fig. 12 gives a top view of the three different layers in Fig. 11. Each cell with a center point represents a red block. The union operation is equivalent to replacing each of the blue center points with the imposed structure between  $\psi_A(\mathbf{r})$  and  $\psi_B(\mathbf{r})$  which also reduced the scale by a half.

The union operation can be looked upon as a special case of the masking operation where the mask index  $m$  always equals to 2. Apply the union operation defined in Eq. (11), we receive:

1. If  $\psi_A(\mathbf{r})$  is a simple basic feature and  $\psi_B(\mathbf{r})$  is a base-centered basic feature,

$$T_{un}[\psi_A(\mathbf{r}), \psi_B(\mathbf{r})] = T_{scal}[\psi_B(\mathbf{r}), 2, 2, 2].$$

2. If  $\psi_A(\mathbf{r})$  is a simple basic feature and  $\psi_B(\mathbf{r})$  is a face-centered basic feature,

$$T_{un}[\psi_A(\mathbf{r}), \psi_B(\mathbf{r})] = T_{scal}[\psi_B(\mathbf{r}), 2, 2, 2].$$

3. If  $\psi_A(\mathbf{r})$  is a base-centered basic feature and  $\psi_B(\mathbf{r})$  is a face-centered basic feature,

$$T_{un}[\psi_A(\mathbf{r}), \psi_B(\mathbf{r})] = T_{scal}[\psi_B(\mathbf{r}), 2, 2, 2].$$

4. If  $\psi_A(\mathbf{r})$  is a simple basic feature and  $\psi_B(\mathbf{r})$  is a body-centered feature,

$$T_{un}[\psi_A(\mathbf{r}), \psi_B(\mathbf{r})] = T_{mask}[\psi_C(\mathbf{r}), \psi_B(\mathbf{r}), 2]$$

where  $\psi_C(\mathbf{r})$  is a face-centered basic feature in the same category as  $\psi_A(\mathbf{r})$  and  $\psi_B(\mathbf{r})$ .

Fig. 13 illustrates the effect of the union operation between the simple cubic and the body-centered basic features.

5. If  $\psi_A(\mathbf{r})$  is a body-centered basic feature and  $\psi_B(\mathbf{r})$  is a face-centered basic feature,

$$T_{un}[\psi_A(\mathbf{r}), \psi_B(\mathbf{r})] = T_{mask}[\psi_B(\mathbf{r}), T_{imp}[\psi_A(\mathbf{r}), \psi_B(\mathbf{r})], 2].$$

Fig. 14 illustrates the effect of the union operation between these two basic features.

6. If  $\psi_A(\mathbf{r})$  is a base-centered basic feature and  $\psi_B(\mathbf{r})$  is a body-centered basic feature,

$$T_{un}[\psi_A(\mathbf{r}), \psi_B(\mathbf{r})] := T_{mask}[\psi_C(\mathbf{r}), T_{imp}[\psi_A(\mathbf{r}), \psi_B(\mathbf{r})], 2]$$

where  $\psi_C(\mathbf{r})$  is a face-centered basic feature in the same category as  $\psi_A(\mathbf{r})$  and  $\psi_B(\mathbf{r})$ .

Fig. 15 illustrates the effect of the union operation between these two basic features.

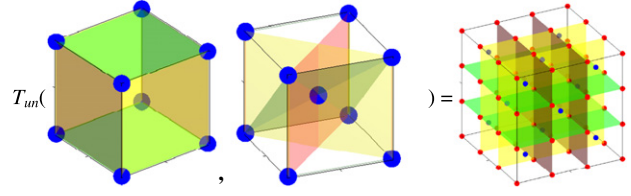


Fig. 13. A simple cubic union with a body-centered cubic.

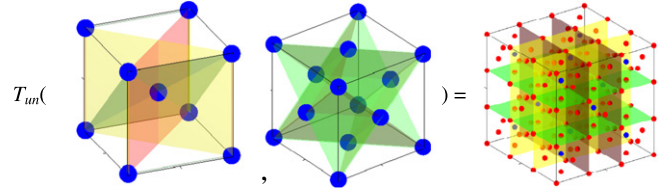


Fig. 14. A body-centered cubic union with a face-centered cubic.

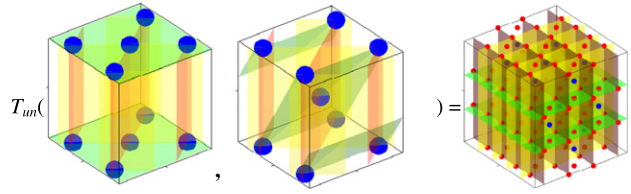


Fig. 15. A base-centered orthorhombic union with a body-centered orthorhombic.

**Lemma 4.** Scaling a unioned structure is equivalent to the union of two features after scaling them first.

**Proof.**

$$\begin{aligned} T_{scal}[T_{un}[\psi_A(\mathbf{r}), \psi_B(\mathbf{r})], s_x, s_y, s_z] \\ &= T_{scal}[T_{mask}[\psi_C(\mathbf{r}), T_{imp}[\psi_A(\mathbf{r}), \psi_B(\mathbf{r})], 2], s_x, s_y, s_z] \\ &= T_{mask}[T_{scal}[\psi_C(\mathbf{r}), s_x, s_y, s_z], \\ &\quad T_{scal}[T_{imp}[\psi_A(\mathbf{r}), \psi_B(\mathbf{r})], s_x, s_y, s_z], 2] \\ &= T_{mask}[\psi_C(\mathbf{S}^{-1} \cdot \mathbf{r}), T_{imp}[T_{scal}[\psi_A(\mathbf{r}), s_x, s_y, s_z], \\ &\quad T_{scal}[\psi_B(\mathbf{r}), s_x, s_y, s_z]], 2] \\ &= T_{mask}[\psi_C(\mathbf{S}^{-1} \cdot \mathbf{r}), T_{imp}[\psi_A(\mathbf{S}^{-1} \cdot \mathbf{r}), \psi_B(\mathbf{S}^{-1} \cdot \mathbf{r})], 2] \\ &= T_{un}[\psi_A(\mathbf{S}^{-1} \cdot \mathbf{r}), \psi_B(\mathbf{S}^{-1} \cdot \mathbf{r})] \end{aligned}$$

where  $\psi_A(\mathbf{r}) \neq \psi_B(\mathbf{r})$ .

### 5.8. Insertion

The insertion operation also deals with the two basic features in the same category. By insertion, the two basic features are separated layer by layer in the  $x$ -,  $y$ - or  $z$ -axis direction. Fig. 16 shows the effect of the insertion operation in the  $z$  axis. The red block layers are separated by the blue layer after the insertion operation between the red block and the blue block.

Notice that if the structure in Fig. 16 is demasked by the red block, the result of this demasking operation is a tetragonal basic feature where  $c = 2a$  if the red block is not a subset of the blue block. The tetragonal basic feature can also be looked upon as a scaled simple cubic feature in the  $z$ -axis direction. Therefore, we generalize the definition of the insertion operation in the  $z$ -axis direction as follows. If  $\psi_C(\mathbf{r})$  is the simple basic feature,  $\psi_D(\mathbf{r})$  is the body-centered basic feature,  $\psi_E(\mathbf{r})$  is the base-centered basic feature and  $\psi_F(\mathbf{r})$  is the face-centered basic feature in the same category as the basic features  $\psi_A(\mathbf{r})$  and  $\psi_B(\mathbf{r})$  ( $\psi_A(\mathbf{r}) \neq \psi_B(\mathbf{r})$ ), the insertion operation in the  $z$  direction is defined as in Box 1.

$$T_{un}[\psi_A(\mathbf{r}), \psi_B(\mathbf{r})] := \begin{cases} T_{mask}[T_{scal}[\psi_A(\mathbf{r}), 1, 1, 0.5], \psi_B(\mathbf{r}), 1] & \text{if } \psi_A(r) = \psi_C(r) \\ T_{imp}[T_{mask}[T_{scal}[\psi_C(\mathbf{r}), 1, 1, 0.5], \psi_B(\mathbf{r}), 1], T_{tran}[T_{scal}[\psi_C(\mathbf{r}), 1, 1, 0.5], 0, 0, c]] & \text{if } \psi_A(r) = \psi_D(r) \text{ and } \psi_B(r) \neq \psi_C(r) \\ \psi_B(r) & \text{if } \psi_A(r) = \psi_E(r) \text{ and } \psi_B(r) = \psi_F(r) \end{cases}$$

Box I.

$$T_{un}[\psi_A(\mathbf{r}), \psi_B(\mathbf{r})] := \begin{cases} T_{mask}[T_{scal}[\psi_A(\mathbf{r}), 0.5, 1, 1], \psi_B(\mathbf{r}), 1] & \text{if } \psi_A(r) = \psi_C(r) \\ T_{imp}[T_{mask}[T_{scal}[\psi_C(\mathbf{r}), 0.5, 1, 1], \psi_B(\mathbf{r}), 1], T_{tran}[T_{scal}[\psi_C(\mathbf{r}), 0.5, 1, 1], a, 0, 0]] & \text{if } \psi_A(r) = \psi_D(r) \text{ and } \psi_B(r) \neq \psi_C(r) \\ T_{imp}[T_{mask}[T_{scal}[\psi_C(\mathbf{r}), 0.5, 1, 1], \psi_B(\mathbf{r}), 1], T_{tran}[T_{scal}[\psi_C(\mathbf{r}), 0.5, 1, 1], a, 0, 0.5c]] & \text{if } \psi_A(r) = \psi_E(r) \text{ and } \psi_B(r) = \psi_F(r) \end{cases}$$

Box II.

$$T_{un}[\psi_A(\mathbf{r}), \psi_B(\mathbf{r})] := \begin{cases} T_{mask}[T_{scal}[\psi_A(\mathbf{r}), 1, 0.5, 1], \psi_B(\mathbf{r}), 1] & \text{if } \psi_A(r) = \psi_C(r) \\ T_{imp}[T_{mask}[T_{scal}[\psi_C(\mathbf{r}), 1, 0.5, 1], \psi_B(\mathbf{r}), 1], T_{tran}[T_{scal}[\psi_C(\mathbf{r}), 1, 0.5, 1], 0, a, 0]] & \text{if } \psi_A(r) = \psi_D(r) \text{ and } \psi_B(r) \neq \psi_C(r) \\ T_{imp}[T_{mask}[T_{scal}[\psi_C(\mathbf{r}), 1, 0.5, 1], \psi_B(\mathbf{r}), 1], T_{tran}[T_{scal}[\psi_C(\mathbf{r}), 1, 0.5, 1], 0, a, 0.5c]] & \text{if } \psi_A(r) = \psi_E(r) \text{ and } \psi_B(r) = \psi_F(r) \end{cases}$$

Box III.

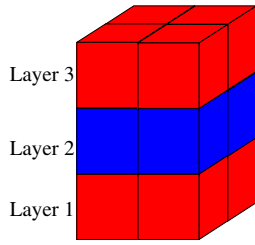


Fig. 16. An illustration of the insertion operation in the z axis.

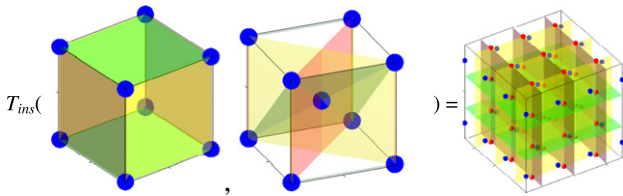


Fig. 17. Insertion between a simple cubic and a body-centered cubic in the z axis.

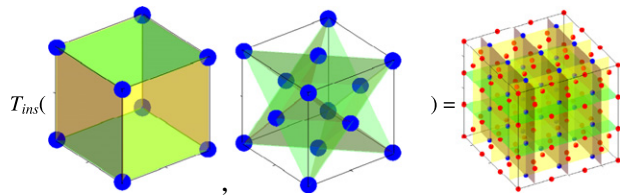


Fig. 18. Insertion between a simple cubic and a face-centered cubic in the z axis.

Fig. 17 illustrates the effect of insertion operation between a simple cubic and a body-centered cubic in the z-axis direction. Fig. 18 illustrates the effect of the insertion operation between a simple cubic and a face-centered cubic. Fig. 19 illustrates the effect of insertion operation between a body-centered cubic and a face-centered cubic.

Insertion operation along x or y axis is similar to its definition in the z axis except when one of  $\psi_A(\mathbf{r})$  and  $\psi_B(\mathbf{r})$  is a base-centered basic feature and the other is a face-centered basic feature. Fig. 20 shows the effect of the insertion operation in the x or y axis.

Similarly, we generalize the definition of the insertion operation in the y-axis direction as follows. If  $\psi_C(\mathbf{r})$  is the simple basic

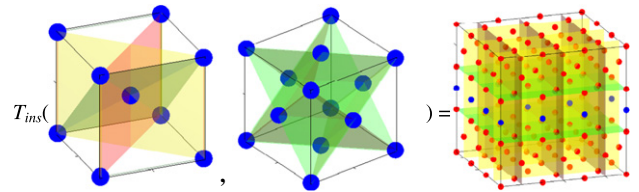


Fig. 19. Insertion between a body-centered cubic and a face-centered cubic in z axis.

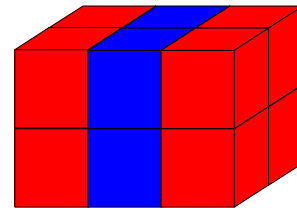


Fig. 20. An illustration of the insertion operation in x or y axis.

feature,  $\psi_D(\mathbf{r})$  is the body-centered basic feature,  $\psi_E(\mathbf{r})$  is the base-centered basic feature and  $\psi_F(\mathbf{r})$  is the face-centered basic feature in the same category as the basic features  $\psi_A(\mathbf{r})$  and  $\psi_B(\mathbf{r})$  ( $\psi_A(\mathbf{r}) \neq \psi_B(\mathbf{r})$ ), the insertion operation along the x axis is defined as in Box II.

The insertion operation along the y axis is defined as in Box III.

## 6. Discussion

The objective of CAND is to open possibility for nanoscientists and engineers to design new materials with desirable properties with the aid of computers. Physical properties are directly determined by structures at nanoscales. Computer-aided design tools to build complex crystal structures are needed. The feature-based approach proposed in this paper provides an alternative method to build crystal structures. The method of feature operations is particularly useful for constructing complex crystal structures such as polycrystalline and superlattice. For example, Si-Ge superlattice is proved to have an electrical conductivity comparable to the SiGe alloy while having a thermal conductivity smaller than that of the alloy [17]. Its unique periodic structure with alternating layers of Si and Ge can be efficiently modeled by

the insertion operation described in Section 5.8. Since complex structures are parametrically modeled with the help of feature-based approach, redesigns and modifications become convenient.

Zero points in the implicit form of our PS model are needed in order to build crystal structures. The computation is based on the discretized space. If each one of the  $x$ ,  $y$  and  $z$  directions is equally divided into  $n$  intervals,  $n^3$  voxel-like cells are created. Thus, zero points are found by searching through all the cells. Those cells whose values are less than a small threshold will be determined as particle positions. Therefore, the time complexity of the feature-based approach is  $O(n^3)$ . This automatic searching process is of advantage over manually specifying positions in the traditional approach.

## 7. Summary

In this paper, rapid construction of crystal structures based on basic features is studied. The basic features, known as fourteen Bravais lattices, are created with the aid of implicit periodic surface models. Several feature operations are defined as an efficient approach to construct complex structures from the basic features. This new feature-based approach provides us an alternative method to build complex crystal structures from basic features and it helps us to generate complex crystal structures efficiently in an interactive CAND environment.

Compared to the existing crystal construction approach that locates the atoms one by one, the feature-based approach enables us to create crystal structures with building blocks. This feature-based approach is helpful if we need to build complex structures because the only inputs from users are parameters of basic features and feature operations. User-defined features can be created based on these operations. Therefore, similar to the feature-based parametric modeling in current CAD systems for macro scale engineering design, the most important advantage of the proposed approach for nanoscale design is to provide an easy-to-use tool to build complex crystal structures.

## Acknowledgement

This work is supported in part by the NSF grant CMMI-0645070.

## References

- [1] Wang Y. Geometric modeling of nano structures with periodic surfaces. Lecture notes in computer science, vol. 4077. 2006. p. 343–56.
- [2] Wang Y. Periodic surface modeling for Computer Aided Nano Design. *Computer-Aided Design* 2007;39(3):179–89.
- [3] Wang Y. Loci periodic surface reconstruction from crystals. *Computer-Aided Design & Applications* 2007;4(1–4):437–47.
- [4] Wang Y. Degree operations on periodic surfaces. In: Proc. 2007 IDETC/CIE conference, 2007 [Paper no. DETC2007-35330].
- [5] Wang Y. Degree elevation and reduction of periodic surfaces. *Computer-Aided Design & Applications* 2008;5(6):841–54.
- [6] Connolly ML. Molecular surfaces: A review. *Network Science* 1996; Available at: <http://www.netsci.org/Science/Compchem/index.html>.
- [7] Lee B, Richards FM. The interpretation of protein structures: Estimation of static accessibility. *Journal of Molecular Biology* 1971;55:379–400.
- [8] Connolly ML. Solvent-accessible surfaces of proteins and nucleic acids. *Science* 1983;221(4612):709–13.
- [9] Carson M. Wavelets and molecular structure. *Journal of Computer Aided Molecular Design* 1996;10:273–83.
- [10] Edelsbrunner H. Deformable smooth surface design. *Discrete & Computational Geometry* 1999;21:87–115.
- [11] Bajaj C, Pascucci V, Shamir A, Holt R, Netravali A. Dynamic maintenance and visualization of molecular surfaces. *Discrete Applied Mathematics* 2003;127: 23–51.
- [12] Au CK, Woo TC. Ribbons: Their geometry and topology. *Computer-Aided Design & Applications* 2004;1(1–4):1–6.
- [13] Ryu J, Kim D, Cho Y, Park R, Kim D-S. Computation of molecular surface using Euclidean Voronoi Diagram. *Computer-Aided Design & Applications* 2005; 2(1–4):439–48.
- [14] Zhang Y, Xu G, Bajaj C. Quality meshing of implicit solvation models of biomolecular structures. *Computer-Aided Geometric Design* 2006;23(6): 510–30.
- [15] Giacovazzo C, Monac HL, Viterbo D, Scordari F, Gilli G, Zanotti G, Catti M. *Fundamental of crystallography*. Oxford Science Publications; 1998.
- [16] Christopher Hammond. *The basic of crystallography and diffraction*. Oxford Science Publications; 1998.
- [17] Lee S-M, Cahill David G, Venkatasubramanian Rama. Thermal conductivity of Si–Ge superlattices. *Applied Physics Letters* 1997;70(22):2957–9.